

Theoretical determination of the necessary conditions for the formation of ZnO nanorings and nanohelices

Z. C. Tu,¹ Q. X. Li,^{1,2} and X. Hu¹

¹*Computational Materials Science Center,*

National Institute for Materials Science, Tsukuba 305-0047, Japan

²*Hefei National Laboratory for Physical Sciences at Microscale,*

University of Science and Technology of China, Hefei, Anhui 230026, P. R. China

Abstract

The formation of ZnO nanorings and nanohelices with large polar surfaces observed in experiments [Nano Lett. **3**, 1625 (2003); J. Am. Chem. Soc. **126**, 6703 (2004)] is shown to be a result of the competition between elastic energy, spontaneous polarization-induced surface energy, volume energy, and defect-induced energy. It is found that nanorings and nanohelices observed in experiments are stable and energetically favorable structures.

PACS numbers: 62.25.+g, 77.65.-j

I. INTRODUCTION

Piezoelectric material produces electrical charges when subjected to pressure, and stretches or contracts when an electrical field is applied,¹ which has been widely used as acoustic transducers in telephones, musical instruments, and so on. Piezoelectric crystals have no center of symmetry, which induces spontaneous polarization.² ZnO is a typical piezoelectric material with Wurtzite structure.³ Zn²⁺ and O²⁻ planes arranging alternately along its *c*-axis results in spontaneous polarization along this direction that induces divergent surface energy of Zn-(0001) and O-(000 $\bar{1}$) surfaces. To maintain them stable, some researchers propose that the surfaces are not reconstructed, in stead about one-fourth charges transfer between them.^{4,5,6} However, theoretical calculation and experiments reveal that the reconstruction is preferable to charge transfer^{7,8} in reducing the surface energy.

After the discovery of ZnO nanobelts,⁹ Kong and Wang synthesized novel ZnO nanobelts, especially, nanorings and nanohelices whose surfaces were dominated by polarized Zn-(0001) and O-(000 $\bar{1}$) facets.¹⁰ They attributed the observed phenomena as a result of surface polar charges and explained that the formation of these nanostructures as a consequence of minimizing the total energy contributed by spontaneous polarization and elasticity.¹⁰ This model requires the ratio of the thickness *t* to the radius *R* of the nanorings to be smaller than a constant, and later more experimental data located in the green domain of Fig.5a in Ref. 11 supported this model. However, the optimal relation between the thickness and the radius of nanorings (black line of Fig.5a in Ref. 11) in their concise model cannot fit well the experimental data. To improve this relation, an elaborate theory considering more factors than their model but remaining its main spirit is needed.

Additionally, because of the symmetry of Wurtzite structure, we know that there are 5 independent elastic constants for bulk ZnO that have been measured as $c_{11} = 190$ GPa, $c_{12} = 110$ GPa, $c_{13} = 90$ GPa, $c_{33} = 196$ GPa, $c_{44} = 39$ GPa.¹² From these experimental values, we see $c_{11} \approx c_{33}$, $c_{12} \approx c_{13}$, and $c_{44} \approx (c_{11} - c_{12})/2$. That is, bulk ZnO can be roughly regarded as an isotropic material, and thus its Young's modulus can be calculated as ~ 120 GPa from these experimental data. It is very surprising that Young's modulus of ZnO nanobelt is measured experimentally only ~ 50 GPa,^{13,14} which is much smaller than that of bulk ZnO. One needs to understand what makes this large difference of Young's modulus between bulk ZnO and the nanobelt.

In the present paper we try to address these issues. The rest of this paper is organized as follows. In Sec. II, we construct the shape formation energy of ZnO nanobelts that consists of elastic energy, spontaneous polarization-induced surface energy, volume energy, and defect-induced energy. And then we put forward necessary conditions of structure existence. In Sec. III, we use necessary conditions of structure existence to explain nanorings and nanohelices observed in experiments. We find that they are stable and energetically favorable structures. In Sec. IV, we give a brief summary and discussion. Some detailed derivations are supplied in Appendix.

II. CONSTRUCTION OF SHAPE FORMATION ENERGY

In order to quantitatively understand morphological problems of nanostructures in theoretical point view, such as helices of multi-walled carbon nanotubes^{15,16} and cholesterol filaments,^{17,18} Ou-Yang and his co-authors proposed a concept that the shape formation energy determines the morphology of structures. Their concept can be summarized and generalized as follows: a structure can exist if its shape formation energy is minimum and less than zero, provided that the thermal fluctuation can be neglected. We will define and construct the shape formation energy of ZnO nanobelts in this section, and then express explicitly the necessary conditions of structure existence.

A. Definition of shape formation energy

The synthesis process of ZnO nanobelts is briefly described as follows.^{10,11} When ZnO powders are heated to 1350 °C at a heating rate of 20 °C/min, they decompose into Zn²⁺ and O²⁻ at low pressure 10⁻³ torr. After a few minutes of evaporation and decomposition, the Ar carrier gas is introduced at a flux of 25 standard cubic centimeters per minute. The condensation products are carried to a temperature zone of 400~500 °C and deposit onto an alumina substrate under the Ar pressure of 250 torr, where the end products—nanobelts are formed. This process can be simplified as a chemical “reaction”:



Schematic energy landscape of the synthesis process of ZnO nanobelts is shown in Fig. 1, where condensation products are regarded as a meso-phase. The shape formation energy F

is defined as the energy difference between ZnO nanobelt and condensation products with the same number of atoms.

A ZnO nanobelt is a thin but long structure as schematically shown in Fig. 2. The symbols + and - represent Zn-terminated and O-terminated surfaces, respectively. The curve C is its central line; \mathbf{e}_1 is the tangent vector of curve C perpendicular to the cross section of the nanobelt; \mathbf{e}_2 and \mathbf{e}_3 (parallel to [0001] direction of ZnO) are principal axes of the cross section. \mathbf{N} is the normal vector of C that determines the bending direction of C in 3-dimensional space, and θ the angle between \mathbf{N} and \mathbf{e}_2 . \mathbf{B} is the binormal vector of curve C . w and t , the width and thickness of the nanobelt because of $w \gg t$ in experiments,^{10,11} represent the dimensions in \mathbf{e}_2 and \mathbf{e}_3 directions, respectively. Because w and t are much smaller than the length of the nanobelt, the geometry of the nanobelt is determined uniquely by its central line C and the angle θ . Since the bending with $\theta = \pm\pi/2$ is preferred to others because of $t \ll w$, we concentrate on this case in this paper. The final form of the shape formation energy of the nanobelt should depend merely on geometric quantities of C , such as the curvature κ and the torsion τ . We propose that it consists of elastic energy, surface energy, volume energy, and defect-induced energy as discussed below.

B. Elastic energy, surface energy, and volume energy

The elastic energy per unit arc length can be written in an invariant quadratic form including infinitesimal displacements of the frame $\{\mathbf{e}_1, \mathbf{e}_2, \mathbf{e}_3\}$:

$$E_c = \frac{k_{12}}{2} \left(\frac{d\mathbf{e}_1}{ds} \cdot \mathbf{e}_2 \right)^2 + \frac{k_{13}}{2} \left[\left(\frac{d\mathbf{e}_1}{ds} \cdot \mathbf{e}_3 \right)^2 + \beta \left(\frac{d\mathbf{e}_2}{ds} \cdot \mathbf{e}_3 \right)^2 \right], \quad (1)$$

where ds is the arc length element. $(d\mathbf{e}_1/ds) \cdot \mathbf{e}_2$ and $(d\mathbf{e}_1/ds) \cdot \mathbf{e}_3$ represent, respectively, the bending deformations around \mathbf{e}_3 and \mathbf{e}_2 , while $(d\mathbf{e}_2/ds) \cdot \mathbf{e}_3$ represents the torsion deformation around \mathbf{e}_1 . $k_{12} = Y_0 t w^3 / 12$, $k_{13} = Y_0 w t^3 / 12$, βk_{13} with $\beta = 2/(1 + \nu)$ are the bending and torsion rigidities,¹⁹ where Y_0 and ν are Young's modulus and poisson ratio of ZnO. For normal materials $0 \leq \nu \leq 1/2$, β is in the range between 4/3 and 2.

Consider the geometric relations $\mathbf{e}_2 = \mathbf{N} \cos \theta - \mathbf{B} \sin \theta$, $\mathbf{e}_3 = \mathbf{N} \sin \theta + \mathbf{B} \cos \theta$, and the

Frenet formula²⁰

$$\begin{pmatrix} d\mathbf{e}_1/ds \\ d\mathbf{N}/ds \\ d\mathbf{B}/ds \end{pmatrix} = \begin{pmatrix} 0 & \kappa & 0 \\ -\kappa & 0 & \tau \\ 0 & -\tau & 0 \end{pmatrix} \begin{pmatrix} \mathbf{e}_1 \\ \mathbf{N} \\ \mathbf{B} \end{pmatrix}, \quad (2)$$

Eq.(1) is simplified as

$$E_c = \frac{k_{13}}{2} [(\alpha \cos^2 \theta + \sin^2 \theta) \kappa^2 + \beta (\tau - d\theta/ds)^2], \quad (3)$$

where $\alpha = k_{12}/k_{13}$. Especially, for $\theta = \pm\pi/2$, the elastic energy per unit arc length can be written as:

$$E_c = \frac{k_c}{2} (\kappa^2 + \beta\tau^2), \quad (4)$$

where $k_c = k_{13} = Y_0 w t^3 / 12$.

Because the nanobelt has two large polar surfaces, we must take into account their surface energy. The surface energy per unit arc length is phenomenologically expressed as

$$E_s = 2\gamma w, \quad (5)$$

where γ is a constant quantity with the dimension of energy per unit area.

The volume energy comes from two sources: One is the Gibbs free energy difference between the solid phase and the meso-phase (condensation products); another is the electric energy induced by the spontaneous polarization. The volume energy per unit arc length is phenomenologically expressed as

$$E_g = g_0 w t, \quad (6)$$

where g_0 is a constant quantity with the dimension of energy per unit volume.

C. Defect-induced energy

As mentioned in Sec. I, the value of experimental Young's modulus of nanobelts (~ 50 GPa) is less than half of bulk ZnO's value (~ 120 GPa). In order to compare the elastic constants of perfect ZnO thin films with bulk ZnO, we adopt a slab model and density functional theory (DFT) method to calculate them.²³ To reduce the computational task, we take the frozen-ion approximation and concentrate on the elastic constant c_{11} . The computed ratio $c_{11}^{slab}/c_{11}^{bulk}$ as a function of the slab thickness is shown in Fig. 3. It is clear that the values of $c_{11}^{slab}/c_{11}^{bulk}$ are close to 1, which implies that the mechanical properties of

perfect ZnO nanobelts have little difference from bulk ZnO. Thus the nanobelts observed in experiments must contain defects that reduce Young's modulus of nanobelts significantly.

There are several clues for the existence of defects in real nanobelts. A direct one is high resolution images of nanobelts. For example, the nanoring shown in Fig.4d of Ref. 10 is not an perfect, uniform structure. High-resolution transmission electron microscopy also reveals that planar defects exist in the nanobelts.^{21,22}

It is hard to write an exact expression of defect-induced energy. But if we only consider structures with $|\kappa t| \ll 1$ and $|\tau t| \ll 1$, the defect-induced energy can be locally expanded up to the second order terms of κt and τt . It is expressed formally as

$$E_d = - [A_1(\kappa t)^2 + A_2(\tau t)^2 + \mu(\kappa t) + A_3] wt, \quad (7)$$

where A_1 , A_2 , A_3 and μ are constant quantities with dimension energy per unit volume. To avoid the symmetry breaking of chirality, the linear term of τt is not included in the above expression. Comparing Eq.(7) with Eqs.(4) and (6), we find that A_1 and A_2 play a similar role with the Young's modulus while A_3 influences the value of volume energy density g_0 . The rest term can induce a local spontaneous curvature of nanobelts randomly. Recently, the idea that defects induce a local spontaneous curvature has also been proposed to explain the cyclization phenomenon of short DNA.²⁴

D. Necessary conditions of structure existence

The final form of the shape formation energy is thus written as

$$\begin{aligned} F &= \int (E_c + E_s + E_g + E_d) ds \\ &= \int \left[\frac{Yt^3}{24}(\kappa^2 + \beta\tau^2) + (2\gamma + gt - \mu t^2\kappa) \right] wds, \end{aligned} \quad (8)$$

where Y and g are the effective Young's modulus and the volume energy density of ZnO nanobelts, respectively. For example, the value of Y can be taken as the experimental value 50 GPa.

Now we estimate the effect of thermal fluctuation on the shapes of nanobelts. Considering the typical growth temperature $T \sim 10^3$ K, the Young's modulus $Y = 50$ GPa, the typical thickness $t \sim 10$ nm, and the width $w > 50$ nm in the experiments,^{10,11} we estimate the persistence length of nanobelts as $l_p = Ywt^3/12T \sim 1$ cm,²⁵ which is much larger than the

typical length of nanobelts of several microns. Thus the effect of thermal fluctuation can be neglected and the necessary conditions of structure existence can be expressed as:

$$\delta F = 0, \quad (9)$$

$$\delta^2 F \geq 0, \quad (10)$$

$$F \leq 0, \quad (11)$$

where δF and $\delta^2 F$ represent the first and second order variations of the shape formation energy, respectively. If a structure satisfies the above three conditions, we call it stable and energetically favorable structure.

From Eq.(9), we arrive at the following shape equations of nanobelts:

$$\kappa_{ss} + \frac{\kappa^3}{2} - \kappa\tau^2 + \frac{\beta}{2} \left[4\tau \left(\frac{\tau_s}{\kappa} \right)_s + \frac{2\tau_s^2}{\kappa} + 3\kappa\tau^2 \right] + \frac{\chi\tau^2}{t} - \frac{(\eta + \xi t)\kappa}{2t^3} = 0, \quad (12)$$

$$2\kappa_s\tau + \kappa\tau_s + \beta \left[\tau_s\tau^2 - (\tau\kappa)_s - \left(\frac{\tau_s}{\kappa} \right)_{ss} \right] - \frac{\chi\tau_s}{t} = 0, \quad (13)$$

where $\chi = 12\mu/Y$, $\eta = 48\gamma/Y$, and $\xi = 24g/Y$. $(\)_s$ represents the derivative respect to s . The detailed derivations of above two equations are shown in Appendix. The necessary conditions of structure existence are transformed into Eqs.(10)–(13).

III. EXPLANATION TO EXPERIMENTS

Now let us use Eqs.(10)–(13) to explain nanorings and nanohelices observed in experiments.

A. Nanorings

For nanorings with radius R , one has $\kappa = 1/R$ and $\tau = 0$. Eq.(12) is transformed into

$$(t/R)^3 = \xi(t/R) + \eta/R, \quad (14)$$

while Eq.(13) is trivial. By fitting this equation to the experimental data¹¹ as shown in Fig. 4, we obtain $\xi = -0.001 \pm 0.0007$ and $\eta = 0.03 \pm 0.01$ nm.

Now we test condition (10). In polar coordinate system (ρ, ϕ) , any perturbation in the vicinity of a cycle with radius R can be expressed as $\rho = R(1 + \sum_{n=-\infty}^{+\infty} a_n e^{in\phi})$, where

$a_{-n} = a_n^*$ ($n = 0, 1, 2, \dots, \infty$) are small constants. The second order variation is evaluated explicitly as

$$\delta^2 F = \sum_n (n^2 - 1)^2 |a_n|^2 Y w t^3 / 12R \geq 0 \quad (15)$$

under the validity of Eq.(14).

Next, nanorings observed in experiments must satisfy condition (11). This requires $F = \pi Y w t^2 (t/R - \chi) / 6 \leq 0$ to be valid for all experimental data. Thus we can take the supremum of t/R in Fig. 4 as the value of χ , i.e., $\chi = 0.08$.

B. Nanohelices

For a nanohelix with radius r_0 and pitch p , the pitch angle is $\varphi = \arctan(p/2\pi r_0)$. The curvature and the torsion are $\kappa = \cos^2 \varphi / r_0$ and $\tau = -\sin \varphi \cos \varphi / r_0$, respectively. Eq.(12) is transformed into

$$\cos^4 \varphi + (3\beta - 2) \sin^2 \varphi \cos^2 \varphi + \frac{2\chi r_0}{t} \sin^2 \varphi = \frac{r_0^2 (\eta + \xi t)}{t^3}, \quad (16)$$

while Eq.(13) is trivial again. Eq.(16) sets a relation between the thickness, the pitch angle and the radius of nanohelices, from which we can estimate the thickness. The results by using the data in Ref. 10 are summarized in Table I. These values are close to the typical value 10 nm observed in experiments.¹⁰

Additionally, the shape formation energy can be calculated as

$$F = \frac{Y w t^3 L}{12r_0^2} \left[\cos^4 \varphi + \frac{2\beta - 1}{4} \sin^2 2\varphi - \frac{\chi r_0}{t} \cos 2\varphi \right], \quad (17)$$

where L is the total length of the nanohelices. Its value is listed in Table I for three nanohelices observed in the experiments using $\chi = 0.08$. Moreover, we also found the matrix

$$\begin{pmatrix} \partial^2 F / \partial r_0^2 & \partial^2 F / \partial r_0 \partial \varphi \\ \partial^2 F / \partial r_0 \partial \varphi & \partial^2 F / \partial \varphi^2 \end{pmatrix}$$

is positive definite for these nanohelices. Therefore, these nanohelices are stable and energetically favorable structures.

IV. CONCLUSION

In the present work, we construct the shape formation energy of ZnO nanobelts that consists of elastic energy, spontaneous polarization-induced surface energy, volume energy, and defect-induced energy. We put forward the necessary conditions of structure existence and find that nanorings and nanohelices of ZnO observed in experiments are stable and energetically favorable structures. We obtain an important result that nanorings and nanohelices must satisfy Eqs.(14) and (16), respectively. We notice that it is easy to measure experimentally the values of the radius of nanorings or the pitch and radius of nanohelices, while it is difficult to measure their thickness of about ten nanometers in high precision because the error of InLens detector is ± 2 nm.^{10,11} Eqs.(14) and (16) provide a way to overcome this difficulty. The present theory may also be developed to explain the recent synthesized superlattice-structured nanohelices.²⁶

Because of the influence of defects, Young's modulus Y and volume energy density g are quite different from the value of perfect and uniform nanobelts. For example, $Y = 50$ GPa is just half of the value of perfect nanobelts. g is estimated as $\sim -10^6$ J/m³ by $\xi = -0.001$. This value departs largely from the cohesive energy $\sim -10^{10}$ J/m³ of ZnO.²⁷ The surface energy density γ is estimated as 0.03 J/m², which cannot compare with the cleavage energy ~ 4 J/m² for perfect Zn-(0001) and O-(000 $\bar{1}$) surfaces obtained by *ab initio* calculations.⁶ There is no theory on the parameter μ at present, which is expected to depend on the defect density and experimental conditions. We estimate its value $\mu \approx 10^8$ J/m³ from the experiment published in Ref. 11.

In the above discussion, we do not include flexoelectric effect^{28,29} of piezoelectric materials in nanoscale. This effect is too small for crystals²⁹ to influence the above results in statics. But it may play a role in the kinetic growth of ZnO nanobelt so that nanorings with Zn-terminated and O-terminated inner surfaces have different weights in the end products. Through analyzing the weights, one may reveal the flexoelectric effect of ZnO in experiments.

Acknowledgement

We are very grateful to Prof. Z. L. Wang, Dr. W. L. Hughes and X. Y. Kong for kindly sending us experimental data. Calculations have been performed on Numerical Materials

Simulator (HITACHI SR11000) at the Computational Materials Science Center, National Institute for Materials Science.

APPENDIX

We present the derivation of Eqs.(12) and (13) from the first order variation of functional (8) under the periodic boundary or fixed boundary. The basic idea is similar to Ref. 30. When we perform the variational calculation, the volume and density of a ZnO nanobelt are allowed to vary, while the total mass is conserved. However, the variation is performed for infinitely small perturbation which has very small effect on the elastic coefficients in Eq.(8). The final Euler-Lagrange equations obtained from the variational process including this effect are the same as those derived from the variation with elastic coefficients fixed to constant.

Let $E_1 = \mathbf{e}_1$, $E_2 = \mathbf{N}$, $E_3 = \mathbf{B}$ and $dE_i = w_{ij}E_j$, where Einstein's summation convention is used and "d" is an exterior differential operator. Thus we have $d\mathbf{r} = E_1 ds$, $w_{12} = \kappa ds$, $w_{13} = 0$, $w_{23} = \tau ds$ by considering the Frenet formula.

First, we consider $\delta\mathbf{r} = \Omega_2 E_2$ and $\delta E_i = \Omega_{ij} E_j$. Using the formula $d\delta\mathbf{r} = \delta d\mathbf{r}$ and $d\delta E_i = \delta dE_i$,³⁰ we have

$$\delta ds = \Omega_2 w_{21} = -\kappa ds \Omega_2, \quad (18)$$

$$\Omega_{12} ds = d\Omega_2, \quad (19)$$

$$\Omega_{13} = \tau \Omega_2, \quad (20)$$

$$\delta w_{ij} = d\Omega_{ij} + \Omega_{ik} w_{kj} - w_{ik} \Omega_{kj}. \quad (21)$$

Because $\delta w_{13} = 0$, we obtain

$$\Omega_{23} ds = [2d(\tau \Omega_2) - \Omega_2 d\tau] / \kappa. \quad (22)$$

Using above five equations, we can prove

$$\delta \kappa ds = d\Omega_{12} + (\kappa^2 - \tau^2) \Omega_2 ds, \quad (23)$$

$$\delta \tau ds = d\Omega_{23} + 2\kappa \tau ds \Omega_2. \quad (24)$$

Considering Stokes theorem and above seven equations, we arrive at

$$\delta \int \kappa^2 ds = \int 2(\kappa_{ss} + \kappa^3/2 - \kappa \tau^2) \Omega_2 ds, \quad (25)$$

$$\delta \int \tau^2 ds = \int \left[4\tau \left(\frac{\tau_s}{\kappa} \right)_s + \frac{2\tau_s^2}{\kappa} + 3\kappa\tau^2 \right] \Omega_2 ds, \quad (26)$$

$$\delta \int \kappa ds = - \int \tau^2 \Omega_2 ds. \quad (27)$$

Consequently, we obtain

$$\begin{aligned} \delta F &= \frac{Ywt^3}{12} \int \left\{ \left(\kappa_{ss} + \frac{\kappa^3}{2} - \kappa\tau^2 \right) + \frac{\beta}{2} \left[4\tau \left(\frac{\tau_s}{\kappa} \right)_s + \frac{2\tau_s^2}{\kappa} + 3\kappa\tau^2 \right] \right\} \Omega_2 ds \\ &+ \int w[\mu t^2 \tau^2 - (2\gamma + gt)] \kappa \Omega_2 ds. \end{aligned} \quad (28)$$

Because Ω_2 is an arbitrary function, $\delta F = 0$ gives Eq.(12).

Secondly, we consider $\delta \mathbf{r} = \Omega_3 E_3$. Using the formula $d\delta \mathbf{r} = \delta d\mathbf{r}$ and $d\delta E_i = \delta dE_i$, we have

$$\delta ds = \Omega_3 w_{31} = 0, \quad (29)$$

$$\Omega_{12} = -\tau \Omega_3, \quad (30)$$

$$\Omega_{13} ds = d\Omega_3, \quad (31)$$

$$\delta w_{ij} = d\Omega_{ij} + \Omega_{ik} w_{kj} - w_{ik} \Omega_{kj}. \quad (32)$$

Because $\delta w_{13} = 0$, we obtain

$$\Omega_{23} ds = [d\Omega_{13} - \tau^2 \Omega_3 ds] / \kappa. \quad (33)$$

Using above five equations, we can prove

$$\delta \kappa ds = -2d(\tau \Omega_3) + \Omega_3 d\tau, \quad (34)$$

$$\delta \tau ds = d\Omega_{23} + \kappa d\Omega_3. \quad (35)$$

Considering Stokes theorem and above seven equations, we arrive at

$$\delta \int \kappa^2 ds = \int (4\kappa_s \tau + 2\kappa \tau_s) \Omega_3 ds, \quad (36)$$

$$\delta \int \tau^2 ds = 2 \int \left[\tau^2 \tau_s - (\tau \kappa)_s - \left(\frac{\tau_s}{\kappa} \right)_{ss} \right] \Omega_3 ds, \quad (37)$$

$$\delta \int \kappa ds = \int \tau_s \Omega_3 ds. \quad (38)$$

Consequently, we obtain

$$\delta F = \frac{Ywt^3}{12} \int \left\{ 2\kappa_s \tau + \kappa \tau_s + \beta \left[\tau_s \tau^2 - (\tau \kappa)_s - \left(\frac{\tau_s}{\kappa} \right)_{ss} \right] - \frac{24\mu \tau_s}{Yt} \right\} \Omega_3 ds. \quad (39)$$

Because Ω_3 is an arbitrary function, $\delta F = 0$ gives Eq.(13).

- ¹ J. F. Nye, *Physical Properties of Crystals* (Clarendon Press, Oxford, 1985).
- ² M. Posternak, A. Baldereschi, and A. Catellani, *Phys. Rev. Lett.* **64**, 1777 (1990).
- ³ Z. L. Wang, *J. Phys.: Condens. Matter* **16**, R829 (2004).
- ⁴ P. W. Tasker, *J. Phys. C* **12**, 4977 (1979).
- ⁵ C. Noguera, *J. Phys.: Condens. Matter* **12**, R367 (2000).
- ⁶ A. Wander, F. Schedin, P. Steadman, A. Norris, R. McGrath, T. S. Turner, G. Thornton, and N. M. Harrison, *Phys. Rev. Lett.* **86**, 3811 (2001).
- ⁷ M. Kunat, St. Gil Girol, Th. Becker, U. Burghaus, and Ch. Wöll, *Phys. Rev. B* **66**, 81402 (2002).
- ⁸ V. Staemmler, K. Fink, B. Meyer, D. Marx, M. Kunat, S. Gil Girol, U. Burghaus, and Ch. Wöll, *Phys. Rev. Lett.* **90**, 106102 (2003).
- ⁹ Z. W. Pan, Z. R. Dai, and Z. L. Wang, *Science* **291**, 1947 (2001).
- ¹⁰ X. Y. Kong and Z. L. Wang, *Nano Lett.* **3**, 1625 (2003).
- ¹¹ W. L. Hughes and Z. L. Wang, *J. Am. Chem. Soc.* **126**, 6703 (2004).
- ¹² T. Azuhata, M. Takesada, T. Yagi, A. Shikanai, SF. Chichibu, K. Torii, A. Nakamura, T. Sota, G. Cantwell, D. B. Eason, C. W. Litton, *J. Appl. Phys.* **94**, 968 (2003).
- ¹³ X. D. Bai et al., *Appl. Phys. Lett.* **82**, 4806 (2003).
- ¹⁴ S. Mao, M. Zhao, and Z. L. Wang, *Appl. Phys. Lett.* **83**, 993 (2003).
- ¹⁵ Ou-Yang Zhong-can, Zhao-Bin Su, and Chui-Lin Wang, *Phys. Rev. Lett.* **78**, 4055 (1997).
- ¹⁶ X. B. Zhang *et al.*, *Europhys. Lett.* **27**, 141 (1994).
- ¹⁷ Shigeyuki Komura, Ou-Yang Zhong-can, *Phys. Rev. Lett.* **81**, 473 (1998).
- ¹⁸ D. S. Chung *et al.*, *Proc. Natl. Acad. Sci. U.S.A.* **90**, 11341 (1993).
- ¹⁹ J. M. Gere and S. P. Timoshenko, *Mechanics of Materials* (Chapman & Hall, London, 1984).
- ²⁰ A. Gray, *Modern Differential Geometry of Curves and Surfaces with Mathematica* (CRC Press, Boca Raton, FL, 1997).
- ²¹ X. Y. Kong, Y. Ding, R. Yang, and Z. L. Wang, *Science* **303**, 1348 (2004).
- ²² Y. Ding, X. Y. Kong, and Z. L. Wang, *Phys. Rev. B* **70**, 235408 (2004).
- ²³ The calculations with DMol³ package [Delley B., *J. Chem. Phys.* **92**, 508 (1990).] use the gen-

eralized gradient approximation with the Perdew-Burke-Ernzerhof for exchange-correlation potential. The basis set consists of the double numerical atomic orbitals augmented by polarization functions. The different thickness of thin film is modeled by periodically repeated slabs containing 2, 4, 6, and 10 Zn-O double layers separated by 10 Å vacuum gaps, respectively. A Monkhorst-Pack grid of $(9 \times 9 \times 9)$ and $(9 \times 9 \times 2)$ k points is used for the bulk unit cell and slab supercell, respectively. The optimized structure parameters of ZnO with Wurtzite structure are $a=3.305$ Å, $c=5.309$ Å, and internal parameter $u=0.380$. Test calculations give the elastic constants of bulk ZnO as $c_{11}^{bulk}=236.8$ GPa, $c_{33}^{bulk}=250.6$ GPa, and $c_{44}^{bulk}=49.9$ GPa, in agreement with the previous theoretical values and experimental results.

- ²⁴ J. Yan, R. Kawamura, and J. F. Marko, Phys. Rev. E **71**, 061905 (2005); P. A. Wiggins and P. C. Nelson, cond-mat/0508155; Y. O. Popov and A. V. Tkachenko, cond-mat/0510302.
- ²⁵ P. G. de Gennes, Scaling Concepts in Polymer Physics (Cornell University Press, New York, 1979); M. Dio and S. F. Edwards, The Theory of Polymer Dynamics (Clarendon Press, Oxford, 1986).
- ²⁶ P. X. Gao, Y. Ding, W. Mai, W. L. Hughes, C. Lao, and Z. L. Wang, Science **309**, 1700 (2005).
- ²⁷ Y. Chen, D. M. Bagnall, H. Koh, K. Park, K. Hiraga, Z. Zhu, and T. Yao, J. Appl. Phys. **84**, 3912 (1998).
- ²⁸ R. B. Meyer, Phys. Rev. Lett. **22**, 918 (1969).
- ²⁹ A. K. Tagantsev, Phys. Rev. B **34**, 5883 (1986).
- ³⁰ Z. C. Tu and Z. C. Ou-Yang, J. Phys. A: Math. Gen. **37**, 11407 (2004).

TABLE I: Radii, pitches, estimated thicknesses and shape energies for different helices. The data for radii and pitches are taken from Ref. 10. L represents the length of helices.

r_0 (nm)	p (nm)	t (nm)	F ($Ywt^3L/12r_0^2$)
342	222	12.4~12.5	-1.1
175	133	8.5~8.6	-0.6
240	380	9.6~9.8	-0.7

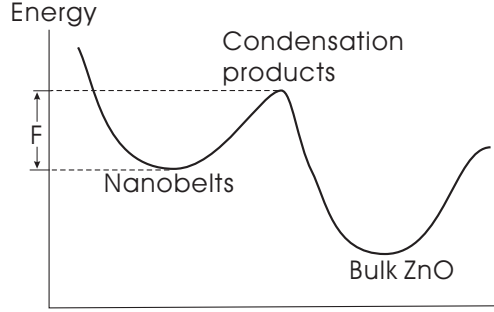


FIG. 1: Schematic energy landscape of the synthesis process of ZnO nanobelts.

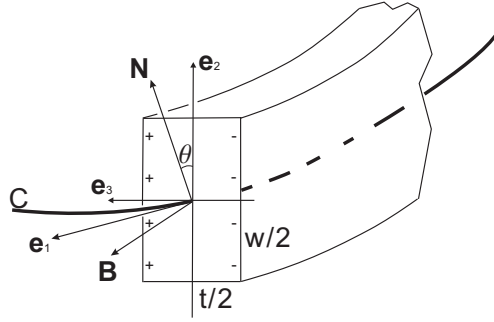


FIG. 2: Schematic figure of a ZnO nanobelt. C represents its central line. \mathbf{e}_1 is the tangent vector of curve C that is perpendicular to the cross section of the nanobelt. \mathbf{e}_2 and \mathbf{e}_3 (parallel to [0001] direction of ZnO) are the principal axes of the cross section. \mathbf{N} and \mathbf{B} are the normal and binormal vectors of C , respectively. θ is the angle between \mathbf{N} and \mathbf{e}_2 .

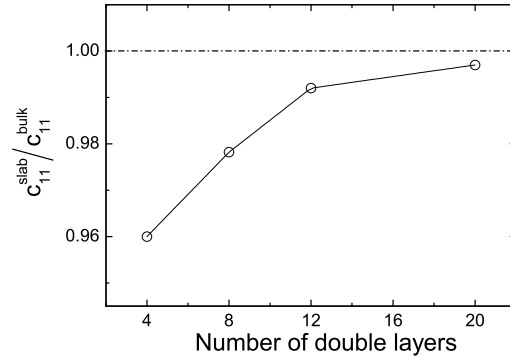


FIG. 3: Relative value of elastic constant c_{11} for a slab and bulk ZnO.

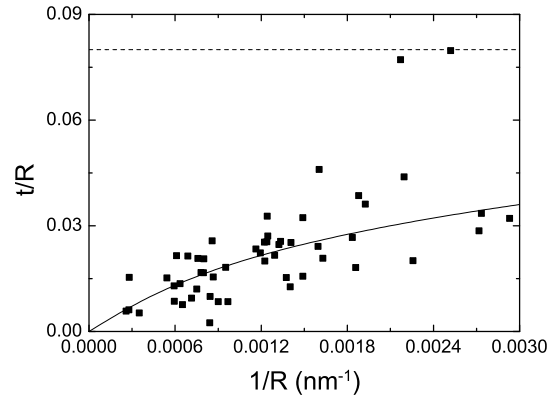


FIG. 4: Relation between $1/R$ and the ratio t/R of nanorings with radius smaller than 4000 nm. The data are taken from Fig.5a of Ref. 11. The solid line is a fitting curve of the data by Eq.(14). The dash line is the supremum of t/R .